Chaos and order in a local barred galaxy model

Haifa Alrebdi[1] and Euaggelos E. Zotos[2]

[1]Princess Nora bint Abdul Rahman University
[2]Aristotle Univ Thessaloniki

February 22, 2024

Abstract

We use an analytical gravitational model that describes the local motion of stars near the central region of a barred galaxy. By integrating and classifying large sets of starting conditions of trajectories we manage to determine how the important parameters of the bar, such as its mass, strength, scale length, and angular velocity influence the motion of stars. For the orbit taxonomy, we combine traditional dynamical methods such as the classical Poincare surface of section along with modern chaos indicators such as the Smaller Alignment Index (SALI). Our results of the local galactic model are compared with previous studies using global gravitational models.

Received 26 April 2000; | Revised 6 June 2000; | Accepted 6 June 2000

DOI: xxx/xxxx

ARTICLE TYPE

Chaos and order in a local barred galaxy model

H. I. Alrebdi[1] | Euaggelos E. Zotos*[2]

[1]Department of Physics, College of Science, Princess Nourah bint Abdulrahman University, P.O.Box 84428, Riyadh 11671, Saudi Arabia
[2]Department of Physics, School of Science, Aristotle University of Thessaloniki, GR-541 24, Thessaloniki, Greece

Correspondence
*Euaggelos E. Zotos Email: evzotos@physics.auth.gr

Present Address
Al. Papadiamanti 1, 48 100, Preveza, Greece

Summary

We use an analytical gravitational model that describes the local motion of stars near the central region of a barred galaxy. By integrating and classifying large sets of starting conditions of trajectories we manage to determine how the important parameters of the bar, such as its mass, strength, scale length, and angular velocity influence the motion of stars. For the orbit taxonomy, we combine traditional dynamical methods such as the classical Poincaré surface of section along with modern chaos indicators such as the Smaller Alignment Index (SALI). Our results of the local galactic model are compared with previous studies using global gravitational models.

KEYWORDS:
Galaxies: kinematics and dynamics – Chaos – Methods: numerical

1 | INTRODUCTION

It is a well-known fact that instabilities in rotating disks usually give birth to barred structures, especially when a massive central mass concentration is absent[1]. Moreover, from an observational point of view, it is estimated that about 67% of spiral galaxies are in fact barred galaxies. Our own Milky Way galaxy along with the neighbor Large Magellanic Cloud are both barred galaxies (see e.g., Refs.[2,3,4]). As for the morphology of the barred structures it varies between large barred structures with extended semi-major axes (of the order of 10 kpc) and weak barred structures with tiny semi-major axes (of the order of 10 pc)[5]. In addition, we can also categorize galactic bars according to their pattern speeds and light profiles. Specifically, we have flat and exponential types of barred structures that usually exist in early-type and late-type barred galaxies, respectively[6].

The vast majority of gravitational models that describe the orbital properties of barred galaxies are in fact mass-models corresponding to the several components of the galaxy, such as the bar, the central bulge, the disk, and the halo[7]. Since the pioneer work of[8] almost all analytical approximations regarding the shape of galactic bars are based on spheroids or ellipsoids (see e.g.,[9]), or logarithmic potentials (see e.g., Ref.[10], or even empirical models obtained through N-body simulations (see e.g., Ref.[11]). All these analytical models have an important common feature that is the effect of the bar's angular velocity on both the properties and also the position of the main orbital resonances[12].

In two earlier works, we numerically investigated the character of orbits in two different types of barred galaxy models. In particular, in[13] we introduced a new gravitational mass-model for barred galaxies, while in[14] we performed an orbit classification in the classical Ferrers' triaxial bar model[8]. Both these models are global models that can describe the motion properties of stars at large galactocentric distances. On the other hand, in[15] they introduced another mass-model for galactic bars which however is a local model and therefore it can replicate the orbital properties of stars relatively close to the central region of the galaxy.

In the present study, we advance the work initiated in[15] by performing a detailed orbit classification for understanding the influence of the bar features (such as mass, strength, scale length, and angular velocity) on the orbits of stars. Our paper has the following structure: Section 2 describes the mathematics of the local model, while the next Section 3 contains all our numerical outcomes. The article ends in Section 4 where we emphasize the main conclusions, while we also compare our results with those of the two earlier papers of [13] and [14].

2 | THE GALACTIC MODEL

Let us briefly remember the model potential introduced in [15].

It is well known, that near the central region of a barred galaxy one can represent the gravitational effects of the nucleus using the potential of a simple harmonic oscillator [2]. Therefore, for modeling the nucleus of the galaxy we adopt the following potential

$$\Phi_n(x, y) = \frac{\upsilon_0^2}{2}\left(x^2 + y^2\right), \tag{1}$$

where υ_0 is a parameter required for the consistency of the units.

The potential of the galactic bar is

$$\Phi_b(x, y) = \frac{-GM_{\rm b}}{\sqrt{x^2 + b^2 y^2 + c_{\rm b}^2}}, \tag{2}$$

where G is the gravitational constant, while $M_{\rm b}$, b, and $c_{\rm b}$ are the mass, the strength, and the scale length of the bar, respectively.

Therefore, the total gravitational potential is $\Phi_t(x, y) = \Phi_n(x, y) + \Phi_b x, y$. Once more, we have to stress out that this total potential applies only locally, near the central region of the galaxy.

Moreover, we assume that the galactic bar rotates, with a constant angular velocity Ω, around the vertical z-axis. This directly implies that in a rotating frame of reference we can use the effective potential

$$\Phi_{\rm eff}(x, y) = \Phi_t(x, y) - \frac{\Omega^2}{2}\left(x^2 + y^2\right). \tag{3}$$

A test particle (star) moves near the central region of the galaxy according to the equations

$$\ddot{x} = -\frac{\partial \Phi_{\rm eff}}{\partial x} - 2\Omega p_y, \tag{4}$$

$$\ddot{y} = -\frac{\partial \Phi_{\rm eff}}{\partial y} + 2\Omega p_x. \tag{5}$$

During the motion of the test particle, its total orbital energy E is conserved, due to the Jacobi integral

$$H = \Phi_{\rm eff}(x, y) + \frac{1}{2}\left(\dot{x}^2 + \dot{y}^2\right) = E. \tag{6}$$

For all the involved parameters, we use the system of galactic units that has been also used in [15]. During our computations the value of υ_0 remains constant at 10, while all the other parameters are treated as variables. However, when $M_{\rm d} = 3000$, $b = 5$, $c_{\rm b} = 1.5$, and $\Omega = 1.25$ we have the so-called *Standard Model* (SM).

3 | MOTION CLASSIFICATION

In what follows we shall demonstrate how the several parameters of the bar affect the motion of the test particle (star) when it moves near the central region of the galaxy. For this purpose, we will construct two-dimensional basin diagrams in which grids each pixel corresponds to a unique set of initial conditions, thus following the pioneer graphical technique of [16,17]. In all cases, the density of the two-dimensional grid is 500×500

All trajectories start with $y_0 = 0$, while the initial value of p_y is always computed through the energy integral (6). Furthermore, the total integration time for all starting conditions is 10^4 time units, using a variable time step.

In our study, the total orbital energy of the test particles remains constant at $E = 250$ which corresponds to a maximum local motion of about 4.5 kpc from the galactic center.

Our aim is to distinguish between chaotic and ordered starting conditions and for this task, we deploy several dynamical tools, such as the classical $(x, \dot{x})$ Poincaré surface of section (PSS), as well as the Smaller Alignment Index (SALI) method [18,19,20]. At the end of the numerical integration, one can determine the nature of a trajectory by inspecting the final value of SALI. Specifically, if SALI $> 10^{-4}$ we have the case of an ordered orbit, while if SALI $< 10^{-8}$ we have the case of a chaotic orbit.

For all the intermediate values where $10^{-8} < \mathrm{SALI} < 10^{-4}$ we have the scenario of a sticky orbit and for this case, additional numerical integration is needed (with higher total time) for unveiling the true chaotic character of the trajectory.

Our preliminary analysis suggests that the orbital structure of the model is very interesting containing a very rich mixture of resonant orbits. In Fig. 1 we present the shapes of the parent periodic orbits of the most important resonant orbits that exist in our local galactic model. Here, it should be explained that for the $n : m$ notation of all resonant orbits we follow the nomenclature of[21].

3.1 | Influence of the mass of the bar

We begin by investigating how the mass of the bar influences the local motion of stars, when $M_{\mathrm{b}} \in [500, 5000]$, while the values of all the other parameters are according to SM. In Fig. 2 (a-f) we preset, for three characteristic values of M_{b}, the corresponding PSSs and the respective distributions of SALI (red colors indicate regular motion, while blue colors correspond to chaotic motion). In the first row of Fig. 2 , where $M_{\mathrm{b}} = 500$, we see that the vast majority of the phase space is covered by starting conditions of regular orbits. A thin chaotic layer is present at the outer regions of the phase plane and contains several embedded islands of secondary resonant motion. In panel (b) of the same figure, it becomes evident that the SALI basin diagram is much more efficient than the classical method of PSS. This is true because we can clearly identify tiny stability regions which are almost invisible in the classical black-and-white PSS. The second row of Fig. 2 corresponds to the SM with $M_{\mathrm{b}} = 3000$. Now we see that the area of the central regular region of 1:1 simple resonant orbits has been reduced, while at the same time the areas corresponding to chaotic motion and secondary resonant orbits have been increased. When $M_{\mathrm{b}} = 5000$, we see at the last row of Fig. 2 that a further reduction of the 1:1 area has occurred, while the regions of secondary resonant orbits have also been reduced, thus giving more room to the unified chaotic sea.

3.2 | Influence of the strength of the bar

We proceed with the next parameter which is the strength of the bar b. Our results are given in the diagrams of Fig. 3 (a-f). In the first row, we present the case of a weak barred structure with $b = 1.5$. It is seen that almost the entire phase plane is occupied by initial conditions corresponding to regular trajectories. Nevertheless, a thin chaotic layer exists mainly at the central region, while it also encircles the invariant curves of the 1:1 resonance. The second row displays again (for comparison reasons) the standard model, in which $b = 5$. In this case, the chaotic regions are much more extended, while a plethora of islands of secondary resonances is present, inside the chaotic regions. The third row corresponds to the scenario of a strong bar with $b = 8$, where the increase of the chaotic reasons has a result the reduction of the areas corresponding to secondary resonant orbits. In general terms, we may conclude that the influence of the strength of the bar follows a similar pattern as the mass of the bar that was already discussed in the previous subsection. In other words, the percentage of chaos increases with increasing mass and strength of the bar.

3.3 | Influence of the scale length of the bar

In the diagrams of Fig. 4 (a-f) we provide the information on how the scale length c_{b} of the bar influences the regular or chaotic character of the orbits of the stars. The first row corresponds to $c_{\mathrm{b}} = 0.5$, that is a case of a rather dense and compact bared structure. We see, that chaos prevails, as it covers more than 70% of the phase plane. The only surviving regular orbits are the simple 1:1 and some additional secondary resonances. On the other hand, the outcomes are completely different when $c_{\mathrm{b}} = 3$ (third row), that is a case of a very loose barred structure. The PSS in panel (e) of Fig. 4 suggests that the entire phase plane is dominated by starting conditions of regular trajectories. However, the SALI basin diagram of panel (f) of the same figure indicates that some extremely weak chaotic layers (corresponding to separatrix structures) are still present. Nevertheless, we may conclude that dense barred structures correspond to highly chaotic phase spaces, while in the case of loose barred structures almost all starting conditions lead to regular trajectories. Moreover, we should also note that in the case of dense galactic bars stars may develop high velocities, mainly approaching the central region, while in the case of loose bars the corresponding velocities are much lower.

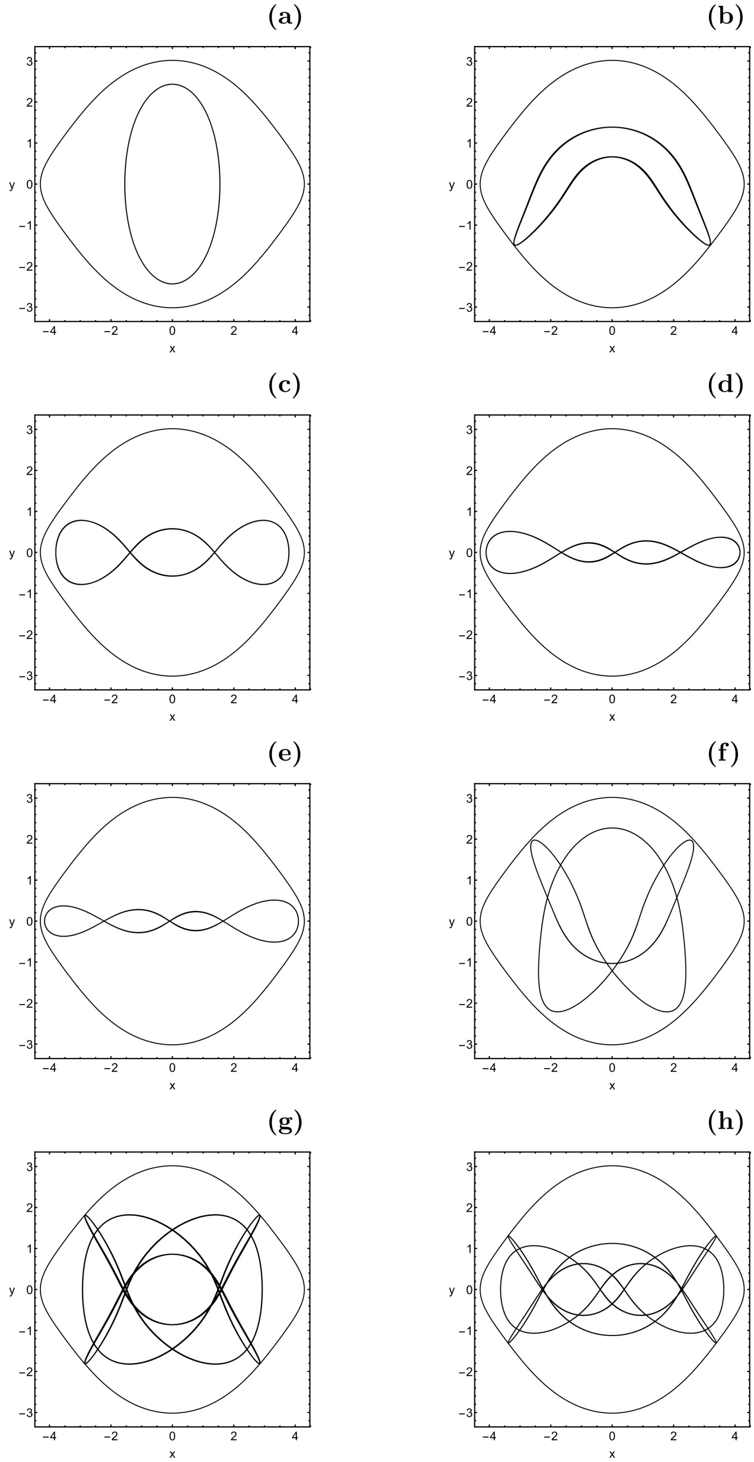

FIGURE 1 Collection of characteristic parent resonant periodic orbits that appear in SM. (a): 1:1, (b): 1:2, (c): 1:3, (d): 1:4, (e): 1:4, (f): 2:3, (g): 3:5, and (h): 3:7. The outermost solid line is the curve of zero velocity.

3.4 | Influence of the angular velocity of the bar

The last parameter under investigation is the angular velocity of the bar Ω. In Fig. 5 (a-f) we present the structure of the phase space for three characteristic values of Ω. In the first row, we have the scenario of a slow rotating bar with $\Omega = 0.1$, where we see that about 80% of the phase plane corresponds to regular motion, while chaos is confined to a chaotic layer surrounding the

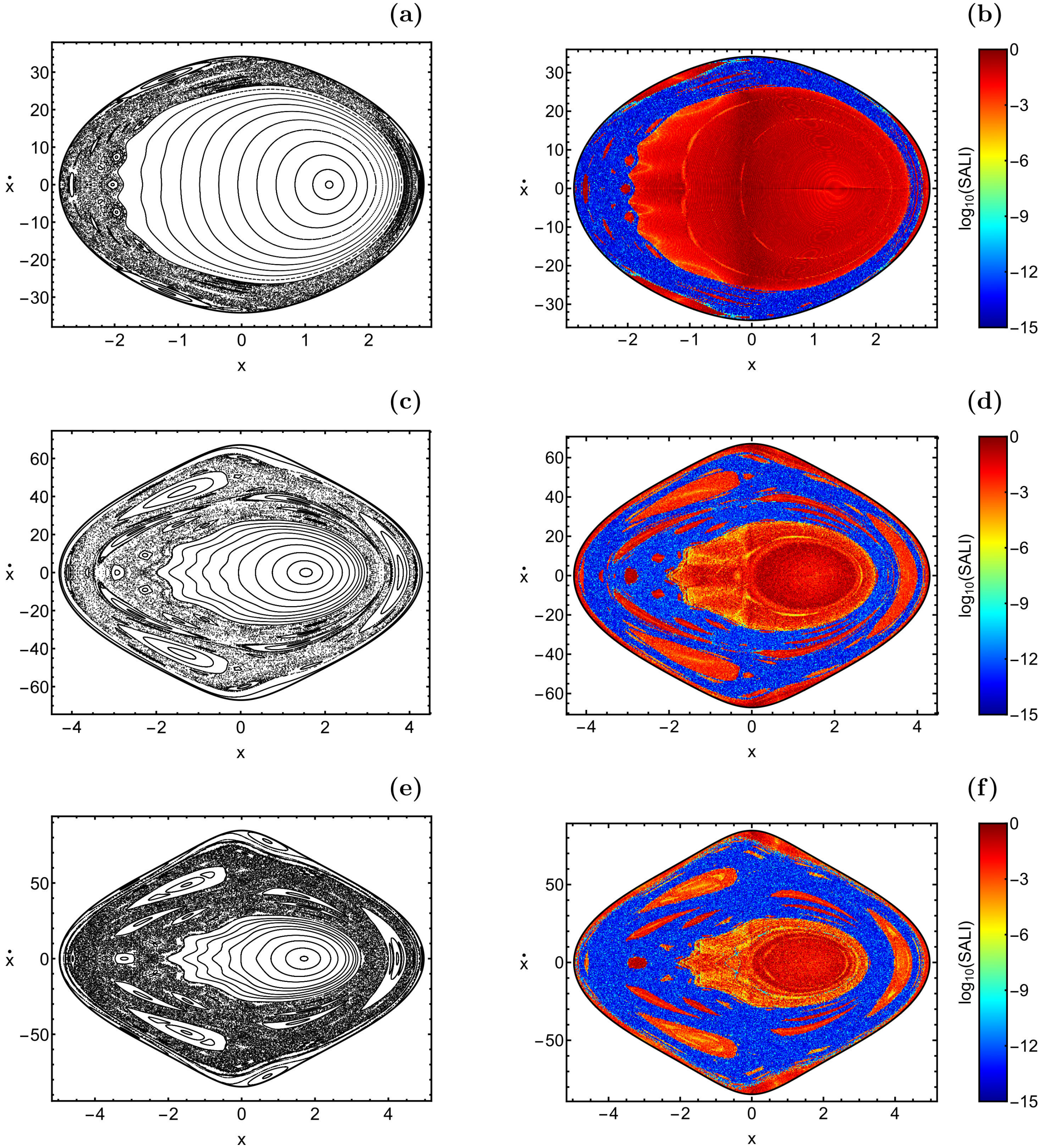

FIGURE 2 Diagrams showing the influence of the mass of the bar M_b. (Left): PSS and (right): the corresponding SALI distributions. (First row): $M_b = 500$, (second row): $M_b = 3000$ (SM), and (third row): $M_b = 5000$.

1:1 resonant orbits. Things however are quite different in the third row which corresponds to the case with a fast rotating bar with $\Omega = 3$. Now the percentages have almost reversed and about 65% of the phase plane is covered by a unified chaotic sea, while regular motion corresponds to the basic resonant orbits. Thus, we may conclude that the angular velocity of the galactic

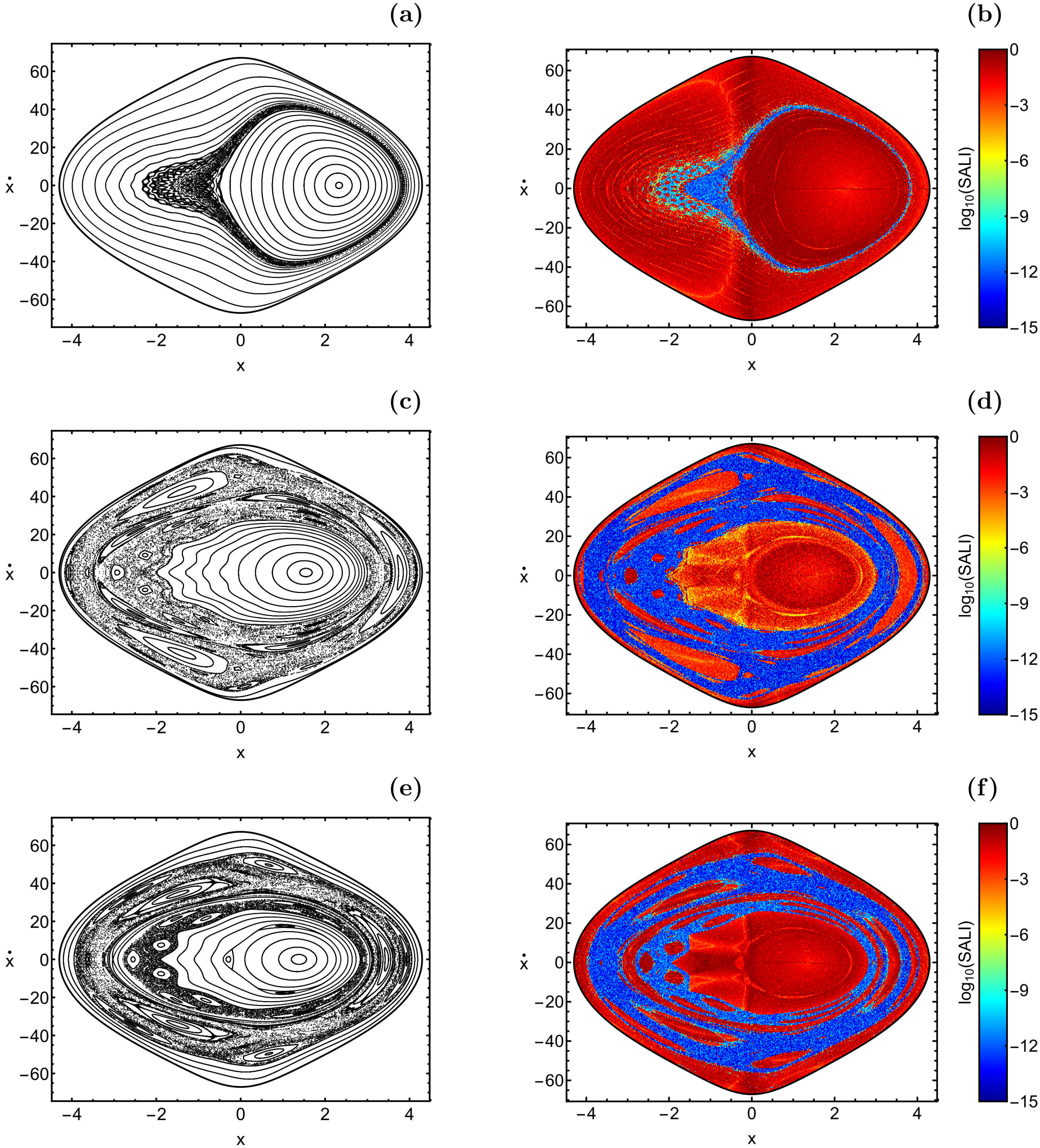

FIGURE 3 Diagrams showing the influence of the strength of the bar b. (Left): PSS and (right): the corresponding SALI distributions. (First row): $b = 1.5$, (second row): $b = 5$ (SM), and (third row): $b = 8$.

bar has a profound influence on the motion of stars. Specifically, as the rotational speed increases the chaotic percentage of the phase space increases significantly.

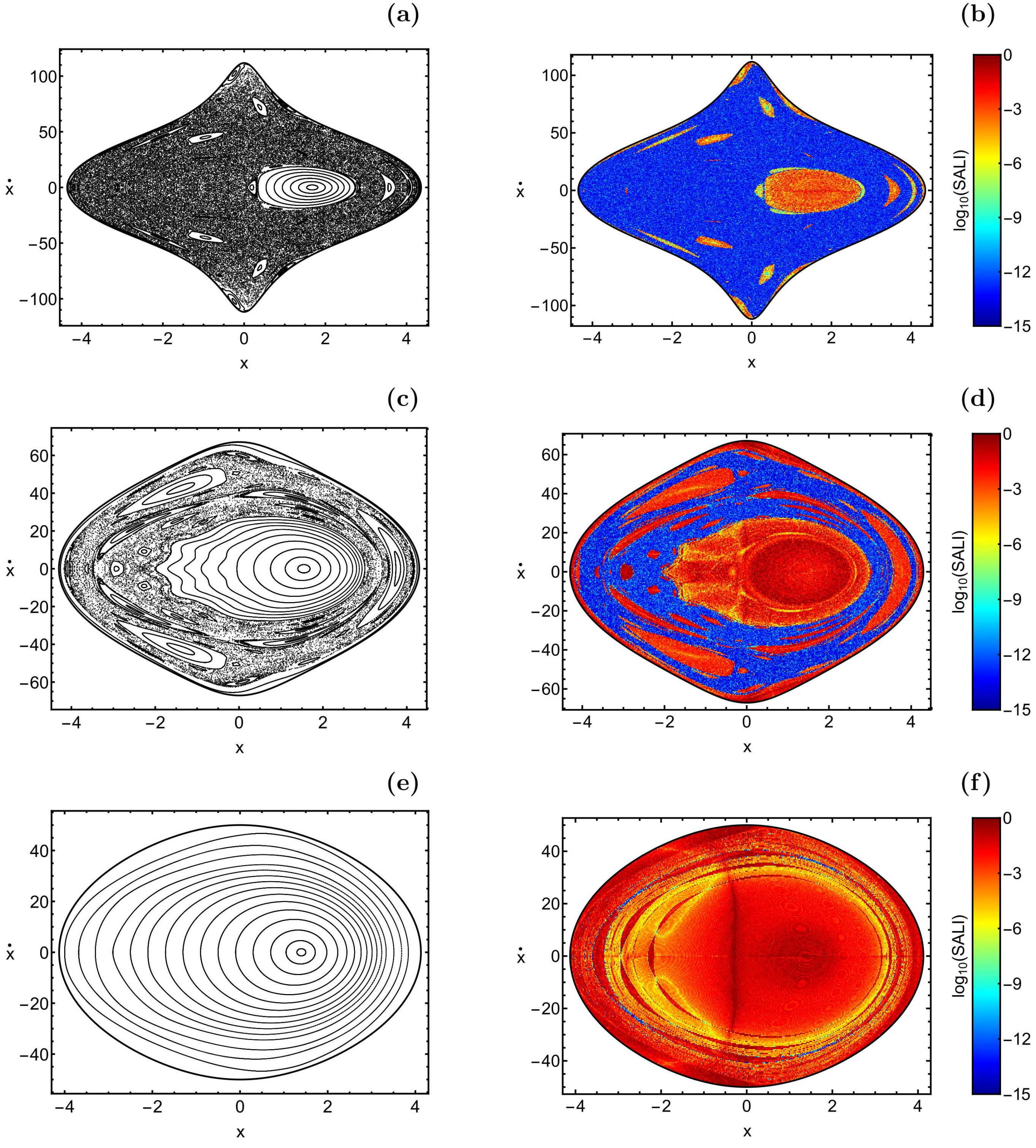

FIGURE 4 Diagrams showing the influence of the scale length of the bar c_{b}. (Left): PSS and (right): the corresponding SALI distributions. (First row): $c_{\mathrm{b}} = 0.5$, (second row): $c_{\mathrm{b}} = 1.5$ (SM), and (third row): $c_{\mathrm{b}} = 3$.

3.5 | Overview analysis

The diagrams presented in the previous subsections correspond to specific values of the parameters associated with the properties of the galactic bar. However, in order to obtain a more complete view on how these parameters affect the local motion of stars we

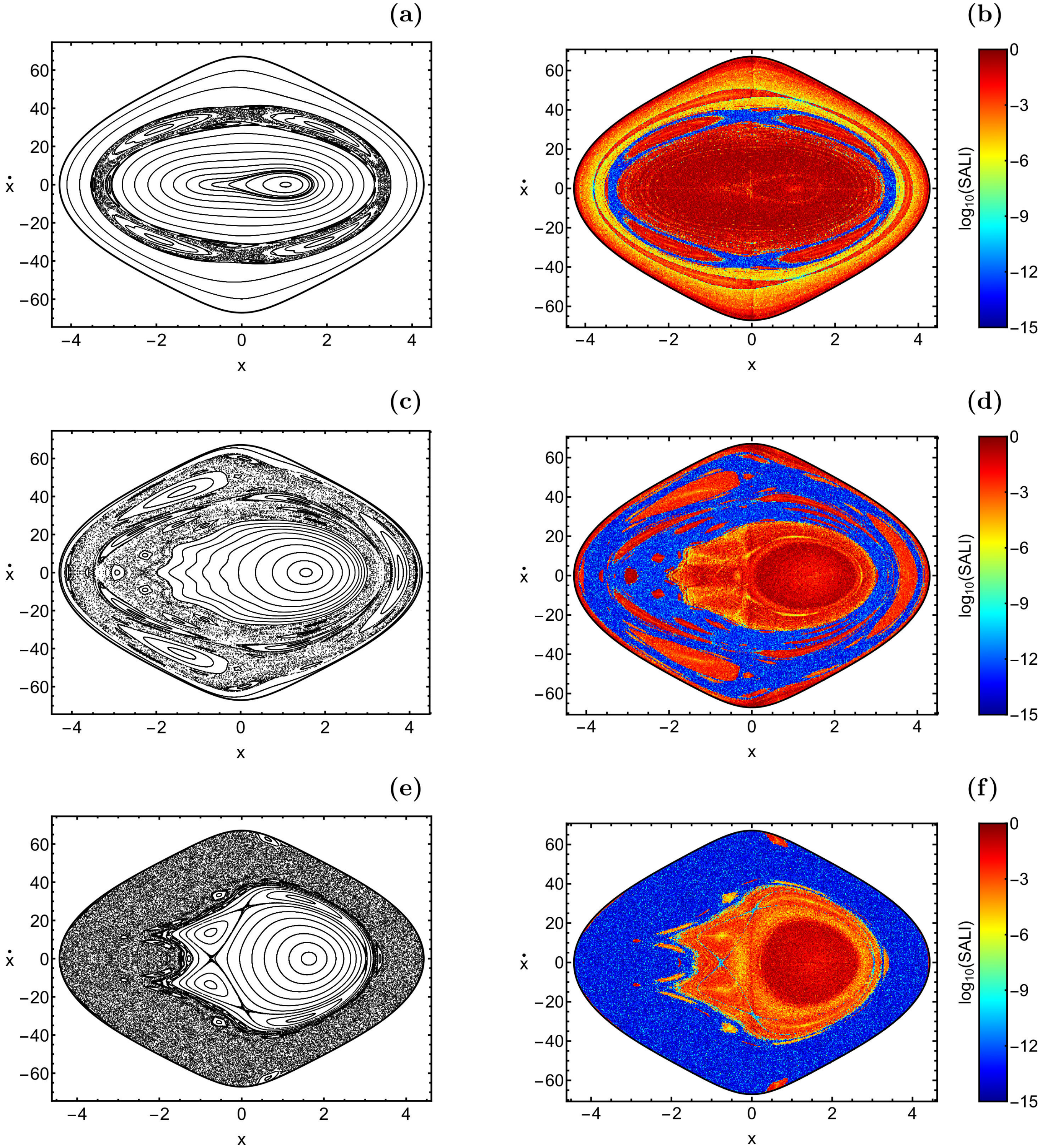

FIGURE 5 Diagrams showing the influence of the angular velocity of the bar Ω. (Left): PSS and (right): the corresponding SALI distributions. (First row): $\Omega = 0.1$, (second row): $\Omega = 1.25$ (SM), and (third row): $\Omega = 3$.

need to study a continuous spectrum of values. Therefore, in Fig. 6 (a-d) we present the nature of trajectories with $y_0 = \dot{x}_0 = 0$, with $\dot{y}_0 > 0$, when $M_b \in [500, 5000]$, $b \in [1, 8]$, $c_b \in [0.5, 3]$, and $\Omega \in [0.1, 3]$.

In the diagram of panel (a) of Fig. 6 we see that for relatively low value of the mass of the bar regular motion dominates. With increasing value of M_b the region between $-2 < x < 2.5$ remains regular, containing the stability islands of 1:1 resonant orbits.

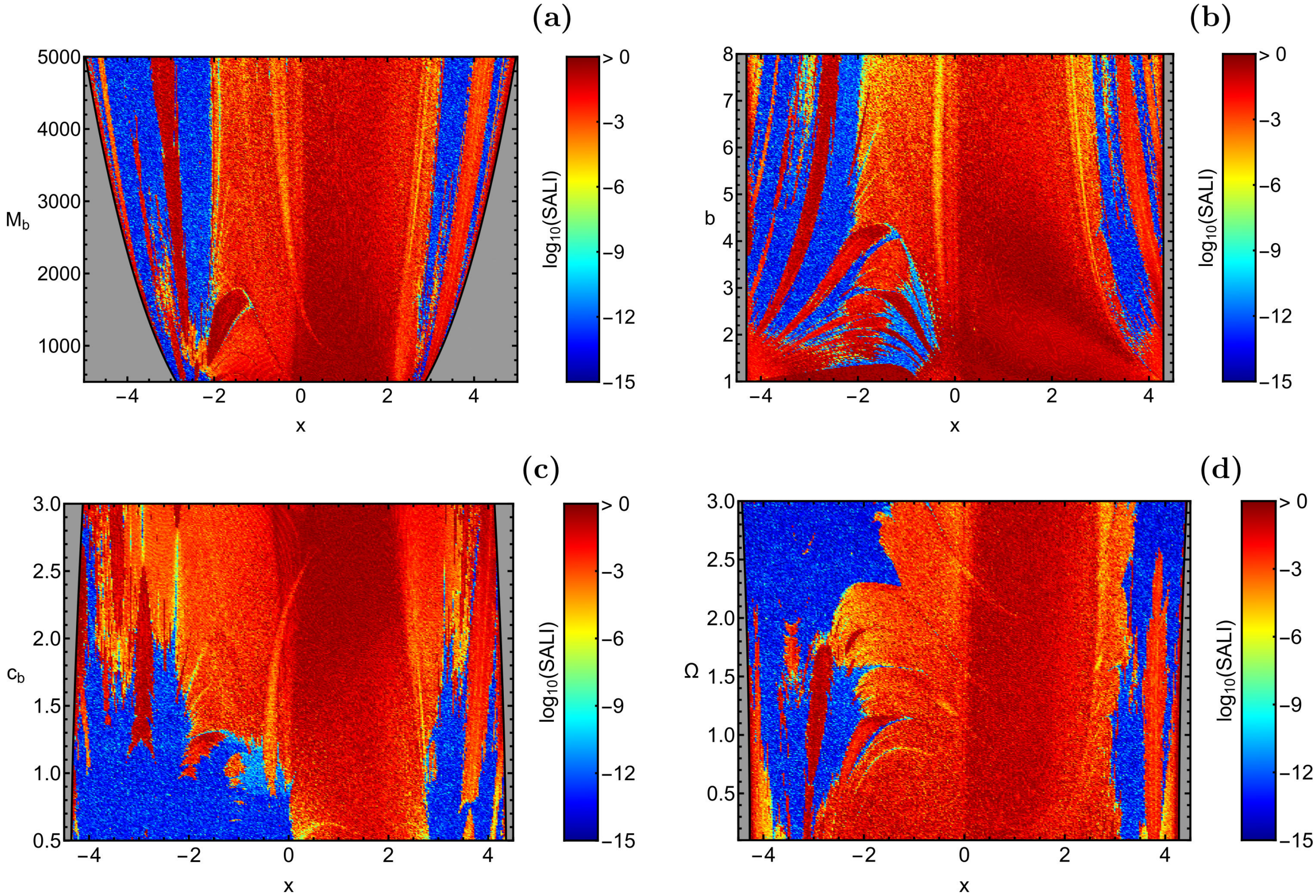

FIGURE 6 Diagrams showing the influence of the (a): mass M_b, (b): strength b, (c): scale length c_b, and (d): angular velocity Ω of the bar, on trajectories starting from the x-axis with $y_0 = \dot{x}_0 = 0$, and $\dot{y}_0 > 0$.

However, near the two edges of the phase space, chaotic regions emerge, and the respective areas grow with increasing value of M_b. We should also point out that the mass of the bar has also an effect on the zero-velocity. Specifically, the energetically allowed region of motion increases as the galactic bar gains mass.

In panel (b) of the same figure, we see that when $b = 1$ the entire phase space is regular due to the integrability of the system. The first indication of chaos appears at about $b = 1.2$ and then chaos is always present through the limit $b = 8$. Furthermore, the chaos evolution in panels (c) and (d) is almost opposite

Looking at all four diagrams of Fig. 6 one can deduce the fact that the type of motion inside the region with $0 < x < 2.5$ seems to be almost unaffected by the change of the values of the bar parameters. Indeed, inside this region, all starting conditions correspond to regular 1:1 resonant orbits, regardless of the values of the involved parameters.

Finally, in Fig. 7 (a-d) we display the evolution of the chaotic percentage of the basin diagrams shown in Fig. 6 (a-d). Now it becomes clear how the four bar parameters affect the character of motion of stars. We see that for the mass as well as the scale length of the bar we have an almost monotonous increase or decrease of the chaotic percentage. On the other hand, for the strength of the bar, we see that for $b > 6$ the chaotic percentage seems to saturate at about 22%. Moreover, regarding the angular velocity the chaotic percentage increases when $0.1 < \Omega < 1.2$, then it drop and then it continues its increase, while for $\Omega > 2.3$ it seems to saturates at about 42%.

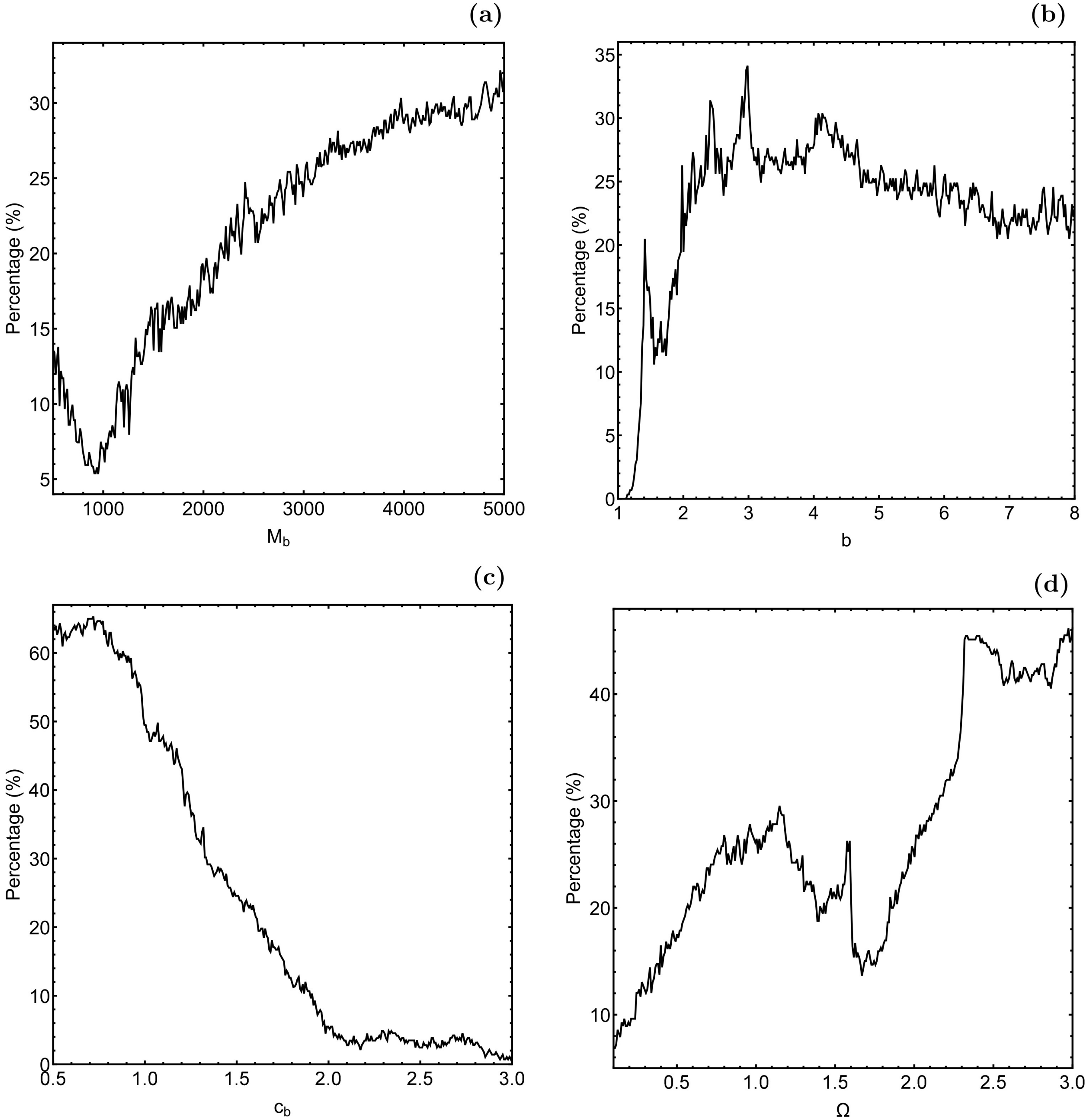

FIGURE 7 Evolution of the chaotic percentage as a function of the (a): mass M_b, (b): strength b, (c): scale length c_b, and (d): angular velocity Ω of the bar. The data correspond to the basin diagrams of Fig. 6 .

4 | DISCUSSION AND CONCLUSIONS

In this study, we adopted the model potential introduced in[15] which consists of a simple harmonic oscillator for the central nucleus and a mass-model for the galactic bar. This model is a local model and can describe the motion of stars moving in the near vicinity of the central region of a barred galaxy. Our aim was to elucidate how the most important parameters of the bar, such as its mass, strength, scale length, and angular velocity influence the local motion of stars. For this task, we integrated and classified large sets of starting conditions of orbits. Specifically, for the orbit taxonomy, we combined traditional dynamical methods, such as the classical Poincaré surface of section along with modern chaos indicators, such as the Smaller Alignment Index (SALI).

We concluded to the following results:

- The chaotic percentage increases with increasing mass of the bar. Moreover, light-weighted bars favor simple 1:1 orbits, while higher resonant orbits appear at relatively heavy bars.
- In the same vein, the rate of chaotic orbits increases as the strength of the bar grows. Once more, simple resonant orbits dominate at weak bars, while higher resonant orbits appear mostly at strong bars.
- At dense and compact bars chaos is very prominent, while the motion becomes completely regular at relatively loose barred structures.
- Slow rotating bars favor regular orbits, while the chaotic rate significantly increases at high rotating bars.

The use of SALI allowed us to detect not only small stability islands but also weak chaotic layers (acting as separatrix) that both are hardly visible in a classical PSS. In addition, SALI gave us the ability to determine the KAM limits of the stability islands where usually sticky orbits live, thus corresponding to intermediate values of SALI.

In two previous papers [13] and [14], we also explored the orbital dynamics in barred galaxies, using two different types of model potentials. However, both these potentials were global potentials, while the one used in the current work is a local potential. On this basis, it would be very interesting to check whether the behavior of the involved parameters is the same or not between these models. After comparing the corresponding results (basin diagrams, chaotic percentages, types of motion, etc) we report that all four parameters of the bar act similarly between our local model and the global model of [13]. On the other hand, in the case of the global model of [14] there is one noticeable difference. While the mass and the strength of the bar seem to influence in the same manner the chaotic percentage in our local model and the model of [14], the angular velocity displays a different pattern. In particular, in our local model, we found that the percentage of chaos increases with increasing angular velocity of the bar. This is also the case in the global model of [13]. However, in the global model of [14] the rate of chaos seems to be reduced as the galactic bar gains speed.

It is in our future plans to continue the current work and focus more on the regular trajectories of the system. Specifically, we would like to demonstrate how the parameters of the bar affect the periodic orbits of the system by presenting the complete network of periodic orbits for each case.

ACKNOWLEDGMENTS

This research paper was funded by Princess Nourah bint Abdulrahman University Researchers Supporting Project number (PNURSP2022R106), Princess Nourah bint
Abdulrahman University, Riyadh, Saudi Arabia.

References

1. Knapen J H. *A&G*. 2005;46:6.28
2. Binney J. Tremaine S. *Galactic Dynamics: Second Edition*. Princeton Series in Astrophysics; 2008.
3. Cheung E. Athanassoula E. Masters K L., et.al. *The Astrophysical Journal*. 2013;779:162
4. Yoon Y. Im M. Lee G H. Lee S K. Lim G. *Nature Astronomy*. 2019;3:844
5. Buta R. 1996, *The Morphology of Barred Galaxies*. In International Astronomical Union Colloquium (Vol. 157, pp. 11-22). Cambridge University Press
6. Elmegreen B G. Elmegreen D M. Chromey F R. Hasselbacher D A. Bissell B A. *The Astronomical Journal*. 1996;111:2233.
7. Sellwood J A. Wilkinson A. *Reports on Progress in Physics*. 1993;56:173
8. Ferrers N M. *Q. J. Pure Appl. Math.*. 1877;14:1
9. Mulder, W. A. Hooimeyer, J. R. A. *A&A*. 1984;134:158-170

10. Gerhard O E. Binney J. *MNRAS*. 1985;216:467

11. Sparke L S. Sellwood J A. *MNRAS*. 1987;225:653

12. Contopoulos G. Grosbol P. *Astron. Astrophys. Rev.*. 1989;1:261

13. Jung Ch. Zotos E E. *PASA*. 2015;32:e042

14. Alrebdi H I., Dubeibe F L., Zotos E E. *Astrophysical Journal*. 2021;920:61

15. Caranicolas N D., Papadopoulos N J. *Astron. Nachr.*. 2007;328:556

16. Nagler J. *Phys. Rev. E*. 2004;69:066218.

17. Nagler J. *Phys. Rev. E*. 2005;71:026227.

18. Skokos Ch. *Journal of Physics A*. 2001;34:10029

19. Skokos Ch, Antonopoulos Ch. Bountis T C. Vrahatis M. N. *Progress of Theoretical Physics Supplement*, 2003;150

20. Skokos Ch. Antonopoulos Ch. Bountis T C., Vrahatis M N. *Journal of Physics A*. 2004;37:6269

21. Carpintero D D., Aguilar L A. *MNRAS*. 1998:298:1

$\square$